Ultraviolet Absorption Spectrum of Chlorine Peroxide, ClOOCl

Francis D. Pope,[†] Jaron C. Hansen,[‡] Kyle D. Bayes,* Randall R. Friedl, and Stanley P. Sander
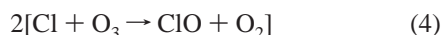
Jet Propulsion Laboratory, California Institute of Technology, Pasadena, California 91109

Received: November 17, 2006; In Final Form: March 6, 2007

The photolysis of chlorine peroxide (ClOOCl) is understood to be a key step in the destruction of polar stratospheric ozone. This study generated and purified ClOOCl in a novel fashion, which resulted in spectra with low impurity levels and high peak absorbances. The ClOOCl was generated by laser photolysis of Cl_2 in the presence of ozone, or by photolysis of ozone in the presence of CF_2Cl_2. The product ClOOCl was collected, along with small amounts of impurities, in a trap at about −125 °C. Gas-phase ultraviolet spectra were recorded using a long path cell and spectrograph/diode array detector as the trap was slowly warmed. The spectrum of ClOOCl could be fit with two Gaussian-like expressions, corresponding to two different electronic transitions, having similar energies but different widths. The energies and band strengths of these two transitions compare favorably with previous ab initio calculations. The cross sections of ClOOCl at wavelengths longer than 300 nm are significantly lower than all previous measurements or estimates. These low cross sections in the photolytically active region of the solar spectrum result in a rate of photolysis of ClOOCl in the stratosphere that is much lower than currently recommended. For conditions representative of the polar vortex (solar zenith angle of 86°, 20 km altitude, and O_3 and temperature profiles measured in March 2000) calculated photolysis rates are a factor of 6 lower than the current JPL/NASA recommendation. This large discrepancy calls into question the completeness of present atmospheric models of polar ozone depletion.

Introduction

The chlorine peroxide molecule, ClOOCl, is formed in the stratosphere when two ClO molecules combine in a three body collision, reaction 1a. This molecule, sometimes referred to as the "ClO dimer" or for this paper just "dimer", participates in the chlorine catalyzed destruction of ozone in the stratosphere.[1] When ClOOCl is photolyzed in the near-ultraviolet, reaction 2,

$$ClO + ClO + M \rightarrow ClOOCl + M \qquad (1a)$$

$$ClOOCl + h\nu \rightarrow ClOO + Cl \qquad (2)$$

$$ClOO + M \rightarrow Cl + O_2 + M \qquad (3)$$

$$2[Cl + O_3 \rightarrow ClO + O_2] \qquad (4)$$

$$\text{Net: } 2O_3 \rightarrow 3O_2$$

it forms Cl + ClOO, rather than ClO + ClO.[2−4] The ClOO radical is marginally stable and usually decomposes to Cl and O_2, reaction 3. These two Cl atoms then can react with ozone, reaction 4, to re-form the two ClO molecules and, in so doing, destroy two O_3 molecules.

Previous studies have identified a strong UV absorption band of ClOOCl with a maximum at about 245 nm and a long tail extending to at least 350 nm.[5−8] Cross sections longer than 300 nm are most important for calculating the photolysis rate of ClOOCl in the atmosphere, because atmospheric ozone eliminates most solar radiation at shorter wavelengths.

Literature values for these long wavelength cross sections vary considerably, by as much as a factor of 5, because of the difficulties in subtracting out the contributions of spectrally featureless impurities such as Cl_2, Cl_2O, Cl_2O_3, and O_3 that are usually present when ClOOCl is generated in the laboratory. Analysis of field measurements of ClO and ClOOCl indicates that the partitioning between these species is consistent with the present understanding of the rate constant for ClOOCl formation only if the largest ClOOCl cross sections[6] are used.[9−12]

The present study reduces the problem of spectral contamination by freezing out the chlorine peroxide and then measuring its absorption spectrum in the gas phase as a function of time as the trap is slowly warmed. Fractionation of the gas stream exiting the trap occurs because of the differences in vapor pressures of different components.

Experimental Methods

A continuous flow of gases only slightly above atmospheric pressure passed through a photolysis cell, a cold trap, an absorption cell and then exited to the hood. The formation of ClOOCl was initiated by laser photolysis in the first cell. The ClOOCl was collected in the cold trap at −120 to −125 °C for 1−2 h. Then the laser and the reactive gases were turned off while the inert carrier gas continued to flow and the trap was rapidly cooled to −150 °C. After about another hour the trap was slowly warmed at a rate of 0.5−1 °C/min, and absorption spectra were recorded every 5.3 s. Significant absorption at 245 nm, due to ClOOCl, began to appear at about −120 °C, reached a maximum at about −115 °C, and approached zero again when the trap reached −90 °C.

* Author for correspondence. E-mail: kdbayes@jpl.nasa.gov. Fax: 818 393 5019. Tel: 818 393 3358.
† Currently at the Centre for Atmospheric Science, Department of Chemistry, University of Cambridge, Lensfield Rd., Cambridge CB2 1EW, United Kingdom.
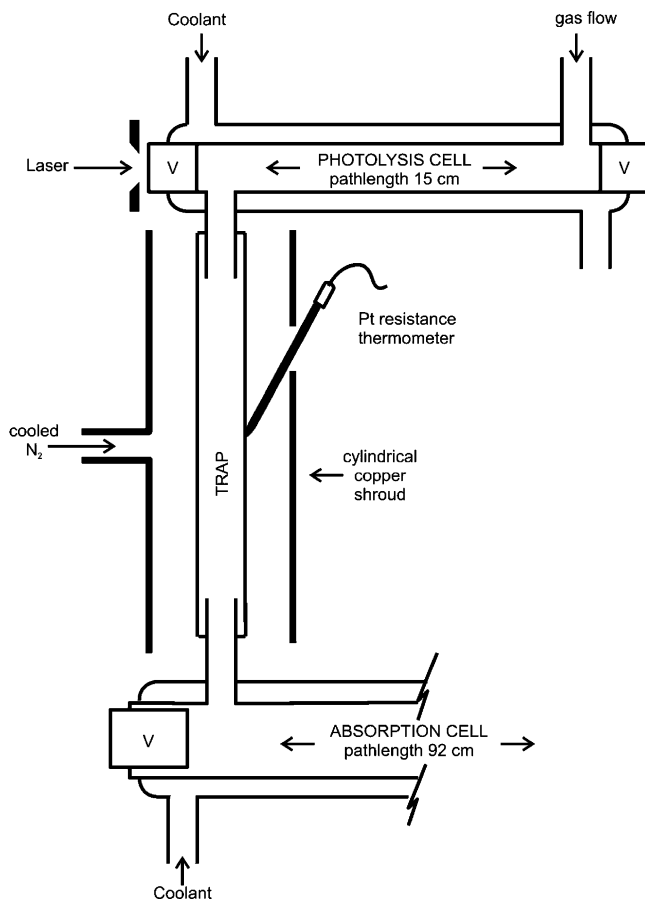‡ Currently at Department of Chemistry and Biochemistry, Brigham Young University, Provo, UT 84602.

UV Absorption Spectrum of ClOOCl

J. Phys. Chem. A, Vol. 111, No. 20, 2007 **4323**

Figure 1. Diagram of the photolysis cell, trap and absorption cell. Quartz was used for all surfaces in contact with the gas stream. V indicates evacuated chambers to avoid water condensation on the windows. The UV analysis beam made two passes through the absorption cell, for a total path length of 184 cm.

Apparatus. A diagram of the quartz photolysis cell and trap is shown in Figure 1. As was observed previously, clean quartz surfaces seemed to be the least destructive of ClOOCl.[7,8] The laser beam entered the photolysis cell at the end nearest the gas exit. A metal ring with a circular opening of 16 mm diameter at the entrance window shielded the sides of the quartz cell from light, minimizing light-piping into the trap. The cell was cooled with circulating methanol at -80 °C. Evacuated spaces at both ends of the cell prevented condensation on the windows, except for humid days when a flow of dry N_2 on the outside windows was also needed. The exit tube of the photolysis cell extended 2 cm into the cold trap to keep the gas stream cold as it passed through the spherical joint region.

The trap was a cylindrical quartz tube, approximately 15 cm in length and 12 mm in internal diameter. The trap temperature was controlled using dry nitrogen that had been cooled by flowing through a coil of copper tubing immersed in liquid nitrogen. The coolant entered through a hole in a metal shroud at the center of the trap and exited to the atmosphere at either end. Increasing the nitrogen flow rate decreased the temperature in the trap. A Pt-resistance thermometer rested against the outside of the trap opposite the cold nitrogen inlet. Thus the reported temperatures only approximately represent those inside the trap.

The absorption cell and optical setup have been described previously.[13] Briefly, a collimated beam from a deuterium lamp (Hamamatsu L1314) traversed the absorption cell twice, giving

a total path length of 184 cm, and then was focused onto the entrance slit of a 0.25 m spectrometer. The dispersed spectrum was detected by a photodiode array (Princeton Instruments, Model PDA-1024H) and stored on a computer. The spectrometer had a 300 line/mm grating with a slit width giving a resolution of about 1 nm FWHM. The wavelength scale was calibrated using mercury lines emitted from a Penray lamp.

The noise level on the absorbance scale was about 0.001 for an integration time of 5 s. However, the baseline on the absorbance scale was not stable over long periods of time. Blank runs with no absorber in the cell showed that the signal was noticeably affected by the temperature cycling of the laboratory air conditioning system. Because the absorbances were determined by measurements of I, during a run, and I_o, which was usually taken at the end of a run, the baseline drift was as much as ± 0.02 absorbance units over a period of 20 min. The baselines were almost independent of wavelength, although some blank runs show a slight nonlinearity at shorter wavelengths. The treatment of the baseline is discussed in the Spectral Analysis section below.

The excimer laser (Lambda Physik, Compex 301) was operated at 351 or 248 nm. The pulse energies were measured at the exit of the photolysis cell with a power meter (Molectron EPM 1000) with only carrier gas flowing through the cell.

Before an experiment began, ozone was generated from pure oxygen using an ozonizer (Welsbach T816) and was trapped on silica gel at -80 °C. During ClOOCl generation, a fraction of the carrier gas was diverted through the ozone trap before entering the photolysis cell. The ozone concentrations were monitored by measuring the absorption of the 254 nm radiation from a mercury Penray lamp after passing through a 1 cm path length cell; the detector was a photomultiplier tube that was band-limited with a narrow interference filter. The partial pressure of O_3 was constant to within 10% during a run.
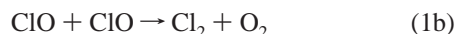
Gas flows were controlled by calibrated flow controllers. The gases used were N_2 (Airgas 99.9993%), He (Airgas 99.999%), O_2 (Airgas 99.8%), 1% Cl_2 in He (Matheson), CF_2Cl_2 (Liquid Carbonic), and CF_4 (Matheson). The total flow rates were typically 1090 sccm during ClOOCl generation and 640 sccm during the desorption phase. The later flow rate, when converted to flows at -80 °C and 730 Torr gave a residence time for the gas in the absorption cell of approximately 90 s.

ClOOCl Generation and Experimental Spectra. Initially our experiments used a low-pressure fast flow system coupled to a quadrupole mass spectrometer[14] to explore the conditions needed to generate, trap out, and transport chlorine peroxide with a minimum of impurities. Clean quartz surfaces were superior to Teflon, halocarbon wax, or Pyrex. Purification by trap-to-trap distillation was attempted, but this did not seem to improve the dimer purity. It was decided to use a minimum of connecting tubing between the generation, trapping and analysis cells, as shown in Figure 1. For measurements of absorption intensity, both a charge coupled device and a photodiode array were used, with the latter proving superior in signal-to-noise.

Spectra were collected on 26 different days. Because the temperature of the trap was controlled manually, no two runs were exactly the same. A major problem was stability of the deuterium lamp and detector, which affected the baseline drift. The analysis of spectra was focused on the five runs that combined strong dimer absorptions, good but not perfect baseline stability, and low impurities.

Two methods were used to generate ClOOCl, one that has been used in previous studies[5,6,8] and a new scheme. These will be discussed separately.

Method 1: $O_3 + Cl_2 + h\nu$(351 nm). A mixture of molecular chlorine and ozone, approximately 0.4 and 3 Torr, respectively, in nitrogen was irradiated with laser pulses of about 40 mJ at 351 nm and 10 Hz. The chlorine atoms that were formed by photolysis of Cl_2 reacted rapidly with ozone to form ClO radicals, reaction 4. For the pressure and temperature used (730 Torr and -80 °C) the ClO + ClO reaction formed primarily ClOOCl (1a); the competing bimolecular channels (reactions 1b, 1c, and 1d) are approximately a thousand times slower for

$$ClO + ClO + M \rightarrow ClOOCl + M \qquad (1a)$$

$$ClO + ClO \rightarrow Cl_2 + O_2 \qquad (1b)$$

$$ClO + ClO \rightarrow ClOO + Cl \qquad (1c)$$

$$ClO + ClO \rightarrow OClO + Cl \qquad (1d)$$

these conditions.[15−18] The gas mixture spent 3.5 s in the photolysis cell and was exposed to 35 laser pulses before exiting to the trap. Modeling showed that the dimer concentration was still increasing after 30 pulses, but at a slower rate because dimer formed by reaction 1a was being destroyed by reaction 5.
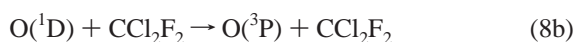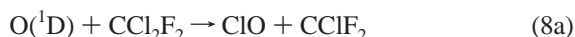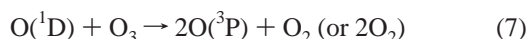
$$Cl + ClOOCl \rightarrow Cl_2 + ClOO \qquad (5)$$
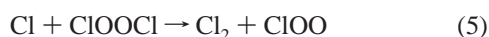
Some dimer could be observed after collecting for only 10 or 15 min, but most runs trapped for periods of 1−2 h, resulting in maximum absorbances ($\ln(I_0/I)$, base e) of 1−3. In addition to the known spectrum of ClOOCl, there was also significant absorption by molecular chlorine. However, as the trap slowly warmed, the chlorine absorption usually peaked before the dimer absorption, indicating some fractionation was taking place.

Especially useful were the spectra taken near the end of the desorption phase. Figure 2 shows five of these spectra. While the ClOOCl absorption is decreasing with time, the Cl_2 peak decreases more rapidly. For the spectra shown in Figure 2 the molecular ratio Cl_2/ClOOCl is decreasing from 2.7 to 1.1 (see Spectral Analysis below). However, for the spectra from method 1, the ratio never went much below unity. Experiments designed to understand the source of this residual Cl_2 signal were inconclusive. Varying the residence time of the ClOOCl in the absorption cell from 2 min to 20 s did not change the final Cl_2/ClOOCl ratio significantly. By intermittently blocking the light coming from the deuterium lamp, we could observe an increase of Cl_2/ClOOCl by about 0.2 when the beam was reintroduced; this effect was largely eliminated by attenuating the intensity of the deuterium lamp. There was no evidence that ozone had been co-deposited with the dimer; this is expected because the vapor pressure of ozone at -125 °C is 340 Torr, well above the amount being used.

Method 2: $CCl_2F_2 + O_3 + h\nu$(248 nm). A new scheme was devised to avoid the presence of large amounts of Cl_2. It is known that when ozone absorbs 248 nm radiation, an excited oxygen atom is formed:[18−20]

$$O_3 + h\nu(248 \text{ nm}) \rightarrow O(^1D) + O_2 \qquad (6)$$
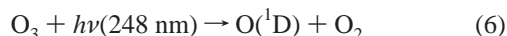
This $O(^1D)$ can then react either with ozone or with CCl_2F_2:

$$O(^1D) + O_3 \rightarrow 2O(^3P) + O_2 \text{ (or } 2O_2) \qquad (7)$$

$$O(^1D) + CCl_2F_2 \rightarrow ClO + CClF_2 \qquad (8a)$$

$$O(^1D) + CCl_2F_2 \rightarrow O(^3P) + CCl_2F_2 \qquad (8b)$$

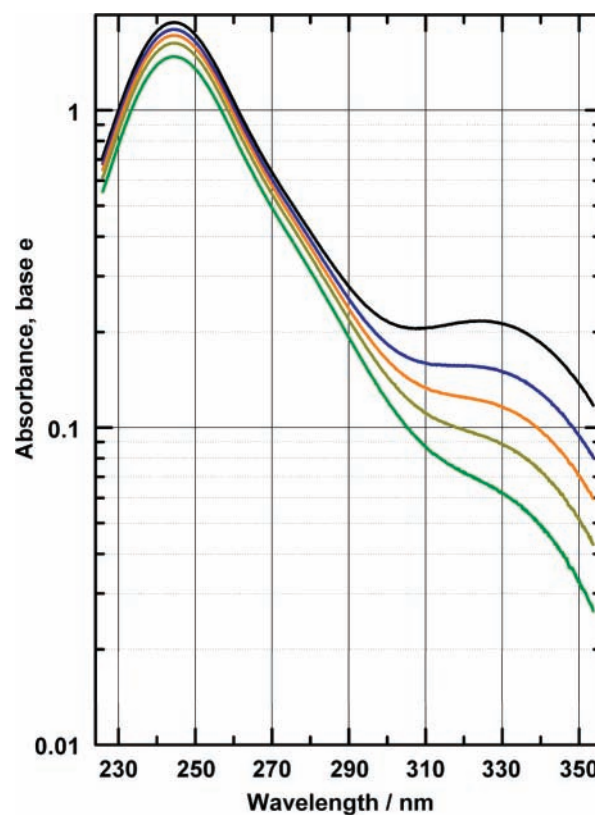Previous studies have shown that approximately 80% of reaction

Figure 2. Absorbance vs wavelength for spectra using method 1 to generate chlorine peroxide. The strong peak near 245 nm is due to ClOOCl and the shoulder at 330 nm is caused by Cl_2. Each spectrum is for a 5 s integration time. These five spectra, with time increasing from top to bottom, were collected during a 2.4 min period.

8 goes by channel 8a, with only 20% deactivation of $O(^1D)$ to the ground state, channel 8b.[21]

For our conditions (2 Torr CF_2Cl_2, 2−3 Torr O_3, balance He, 730 Torr and -80 °C), the chlorodifluoromethyl radicals formed in reaction 8a should react primarily with ozone to form chlorodifluoromethoxy radicals, reaction 9. Methoxy radicals

$$CClF_2 + O_3 \rightarrow ClF_2CO + O_2 \qquad (9)$$

in which there is at least one Cl or Br are known to decompose rapidly by ejecting a halogen atom.[22−25] Because the C−Cl bond is weaker than the C−F bond, one expects reaction 10 to dominate. The resulting Cl atom will then react with ozone to

$$ClF_2CO \rightarrow Cl + CF_2O \qquad (10)$$

form another ClO. Fortunately the UV absorption of the product CF_2O does not interfere with measurements of the ClOOCl spectrum.[26]

This new scheme has the potential to generate ClO dimer with very low amounts of Cl_2. Reaction 5 should be the only significant source of Cl_2. Modeling showed that for the conditions used, the molecular ratio of Cl_2 to ClOOCl would be about 0.06 after one pulse, 0.6 after the second pulse, and 1.4 after the third pulse of 248 nm in the same sample of gas. The very low production of Cl_2 in the first pulse results when Cl atoms formed by the laser are destroyed rapidly by reaction 4, mostly before the slower reaction 1a can form ClOOCl. However, when the second pulse arrives, the new supply of Cl atoms can react with the ClOOCl formed in the first pulse, giving a larger ratio of Cl_2/ClOOCl.
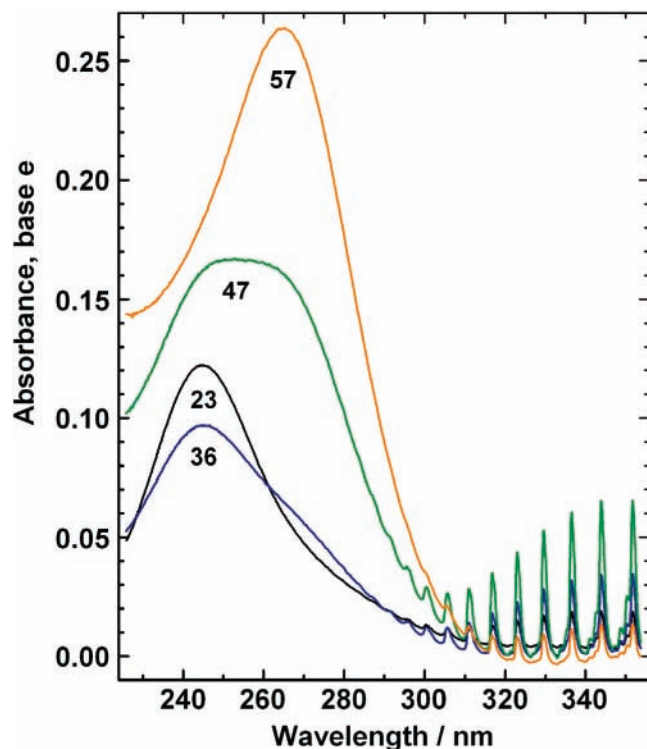
Figure 3. Absorbance vs wavelength for spectra using method 2 to generate ClOOCl. Each spectrum is the average of ten 5 s spectra. The numbers under each peak represent sequential numbering as the trap warms. Conditions: 3 Torr O_3; 1.8 Torr CF_2Cl_2; balance He. The approximate trap temperatures were -119 (spectrum 23), -106 (36), -94 (47), and -82 (57) °C.

The production of Cl_2 by reaction 5 was minimized by limiting the generation of dimer to a single pulse. This was accomplished by running the laser at 1 Hz and using high O_3 concentrations (2$-$3 Torr). Because the cross section of ozone for 248 nm radiation is large (1.1 $\times$ 10^{-17} cm^2), most of the light was absorbed within 2 or 3 cm of the front window. The flow velocity within the photolysis cell was about 4 cm s^{-1}, so most of the irradiated gas flowed into the trap before the next laser pulse. Dumping all of the pulse energy (50 mJ) into a volume of gas of about 6 cm^3 should cause a temperature jump of 10 K; this is not sufficient heating to destroy the dimer before it could reach the trap.

Initial experiments with method 2 used He as the carrier gas, because N_2 deactivates $O(^1D)$ very rapidly. The ClOOCl formation rate was about a factor of 5 less than observed using method 1, but there was clearly less Cl_2 contamination. However, a new problem appeared; there was a strong absorption due to OClO molecules. At first we suspected that the system had been contaminated by water, because an ice surface causes the formation of OClO from ClO.[27] However, extensive drying did not reduce the OClO signal. When a strong OClO absorption was present, the dimer spectrum also was contaminated by Cl_2O_3 due to reaction 11.

$$OClO + ClO + M \rightarrow Cl_2O_3 + M \qquad (11)$$

Once the products had been collected in the trap, the warming and recording of spectra were similar to those used in method 1.

Examples of the spectra observed using method 2 are shown in Figure 3. The numbers on the figure represent sequential spectra, each a 50 s average, during the warming of the trap. The early spectra (e.g., 23) show a peak absorbance at 245 nm

indicating ClOOCl, but with significant OClO evident at wavelengths longer than 300 nm. As the trap warmed, a shoulder builds on the long wavelength side of the 245 nm peak (spectrum 36), and eventually a new peak emerges at about 265 nm (spectrum 57) corresponding to the strong Cl_2O_3 band. The total time covered in Figure 3 is about 1 h.

Because it is known that reaction 8a forms vibrationally hot ClO,[21] the possibility that this extra vibrational energy was responsible for OClO formation was tested by replacing part of the He flow by CF_4, which should be better than He at vibrationally relaxing hot ClO. The (OClO + Cl_2O_3) signal was reduced by a factor of 10 for 21% CF_4. Additional CF_4 up to 71% did not reduce the OClO further.

The reaction responsible for OClO formation is not known. One possibility is that reaction 1d or reaction 12, normally slow,

$$ClO* + O_3 \rightarrow OClO + O_2 \qquad (12)$$
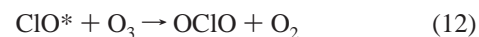
could be accelerated by the extra vibrational energy in the ClO. There was some indication that the OClO formation was greater for the larger ozone concentrations, which would support reaction 12, but this possibility was not pursued further.

Spectral Analysis

Previous attempts to measure the spectrum of ClOOCl have also had to eliminate the contributions of impurities such as Cl_2, Cl_2O, OClO, and Cl_2O_3. Because the spectra of the impurities are known, these were subtracted from the measured absorption in varying amounts until the resulting spectrum looked reasonable. For an impurity such as OClO, which has a series of sharp peaks, this method works well. But for broad spectral features, such as those for Cl_2 or Cl_2O_3, this method becomes quite subjective.

Figure 4 illustrates the uncertainties associated with the subtraction method. The black line in Figure 4 is a spectrum generated using method 1, chosen because it shows a distinct bump near 330 nm due to Cl_2 and also because it extends to longer wavelengths than those in Figure 2. The colored curves in Figure 4 show the results of subtracting increasing amounts of the known Cl_2 spectrum.[28] Which one of the subtractions gives the best representation of the spectrum of pure ClOOCl? Clearly the lowest red curve results from subtracting too much. But beyond rejecting negative absorbances, what criteria can be used to decide on the "best" curve? There is no hint of a bump at 330 nm in any of the colored curves. Should the absorbance of ClOOCl at 360 nm really be zero, or some finite value? How can one decide?

Faced with this problem, Huder and DeMore,[7] after subtracting the obvious Cl_2 bump, decided to extrapolate their curve beyond 310 nm by using a straight line in a plot of log(σ) vs wavelength. However, none of the colored lines in Figure 4 is a good straight line when plotted in this fashion. Also there is no real theoretical justification for a log-linear extrapolation. The decision of how much Cl_2 spectrum to subtract comes down to a personal choice.

We have used a different approach to the problem of spectral subtraction by applying the method of least squares. This method requires an analytical expression for the unknown spectrum and either analytical expressions or recorded spectra for the impurities. For the spectra obtained using method 1, the only obvious impurity was Cl_2. Maric et al. have found that an expression using two Gaussian-like terms is sufficient to describe the Cl_2 spectrum.[28,29] When adjusted to a temperature of -80 °C using their recommended temperature dependence, the cross sections
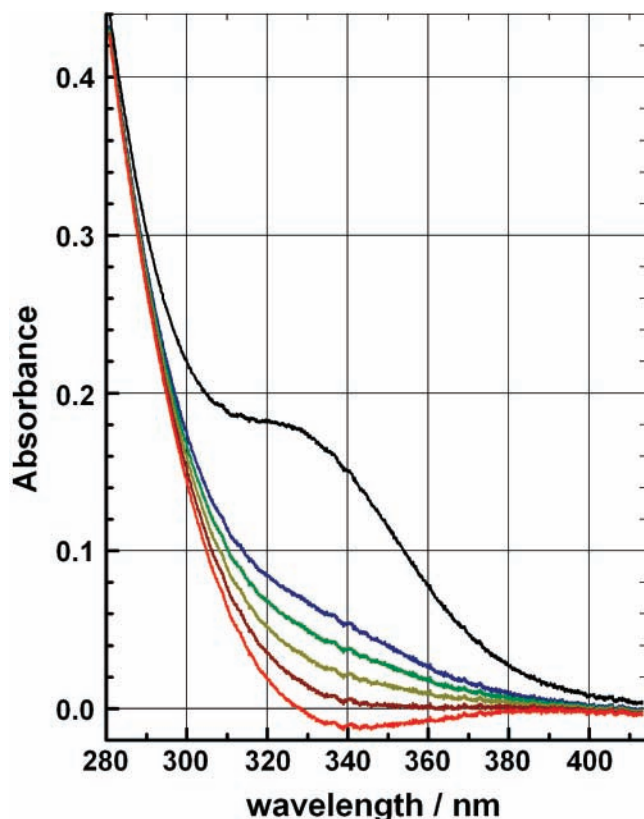
Figure 4. Black line: measured absorbance using method 1 to generate ClOOCl. Colored lines: results of subtracting increasing amounts of the Cl_2 spectrum from black line.
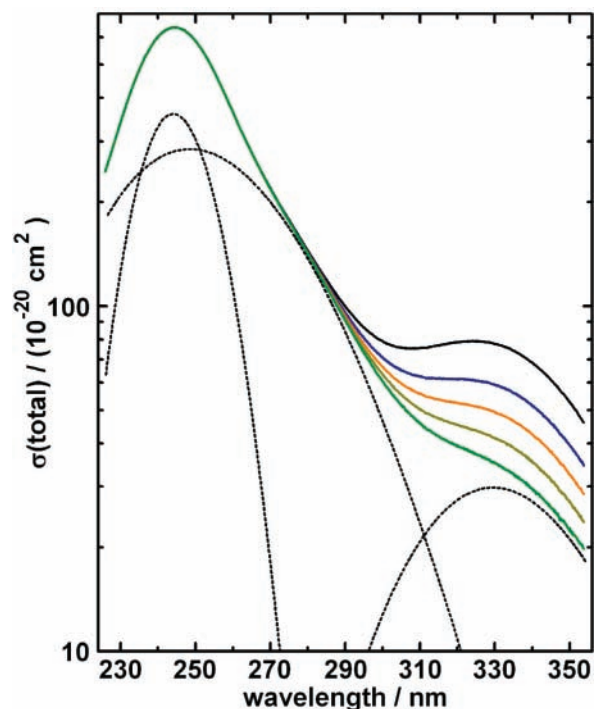

Figure 5. Spectra normalized to 640 at 244.7 nm using eq 15. The five spectra are the same as those shown in Figure 2. The three black dotted curves represent the two Gaussian terms in eq 16 and $\sigma(Cl_2)$ multiplied by 1.107, which is the fitted molecular ratio of Cl_2/ClOOCl for the lowest (green) spectrum.

as a function of wavelength become

$$\sigma(Cl_2) = 26.88 \exp(-96.0[\ln(329.5/\lambda)]^2) +$$
$$0.918 \exp(-88.7[\ln(406.5/\lambda)]^2) \quad (13)$$

where the units of λ are nm and the units of σ are 10^{-20} cm² molecule⁻¹; these units will be used throughout this report. Measurements on a dilute Cl_2/He mixture at -80 °C in our system showed excellent agreement with eq 13.

Maric and co-workers have argued that Gaussian-like expressions similar to those used in eq 13 are the best representation for electronic transitions from bound lower states to repulsive excited states.[28,29] In addition to Cl_2, these expressions have been used to describe spectra of Br_2,[30] BrCl,[29] HOBr,[31] CF_3I,[32] and peroxy radicals.[33-36] Because the electronic transition in ClOOCl is also expected to be of the bound-to-repulsive type, we tried fitting spectra by using a combination of one Gaussian-like term and the above expression for $\sigma(Cl_2)$. The resulting fit was very poor, obviously not the correct form for the ClOOCl spectrum. However, with two Gaussian-like terms, the fit to the measured absorbances, $A(\lambda)$, was excellent. The analytical expression used was eq 14, where the least-squares method fits a total of eight

$$A(\lambda) = a_1 \exp(-w_1[\ln(L_1/\lambda)]^2) +$$
$$a_2 \exp(-w_2[\ln(L_2/\lambda)]^2) + y\sigma(Cl_2) + B \quad (14)$$

parameters, three for each Gaussian (a, w, and L), one (y) to match the amount of Cl_2 present, and a constant term, B, to allow for any nonzero baseline. All least-squares analyses of data were done using the program PSI Plot.

Because we have made no measurements of absolute cross sections, it was necessary to scale our absorbances to previous absolute measurements to report cross sections as a function of wavelength. We have followed the current JPL-NASA recommendation[18] that the peak cross section at 245 nm is 640×10^{-20} cm² molecule⁻¹. This conversion was done using eq 15,

$$\sigma(\text{total}) = \frac{640(A(\lambda) - B)}{(A_{\max} - B)} \quad (15)$$

where $A_{\max}$ represents the maximum numerical value of absorbance in a spectrum, observed to be at 244.7 ± 0.3 nm, and the fitted value for B has been subtracted to eliminate any nonzero baseline. As an example of this procedure, the five spectra in Figure 2 have been replotted as $\sigma(\text{total})$ in Figure 5. It should be noted that the short wavelength portion of these spectra overlap very well when fitted to the same maximum cross section.

These cross sections, all in units of 10^{-20} cm², could be refitted by least squares using eq 16. The amplitude factors, C_1 and C_2, are in the same units as σ, and x now represents the

$$\sigma(\text{total}) = C_1 \exp(-w_1[\ln(L_1/\lambda)]^2) +$$
$$C_2 \exp(-w_2[\ln(L_2/\lambda)]^2) + x\sigma(Cl_2) \quad (16)$$

molecular ratio of Cl_2 to ClOOCl. As expected, the values for w_1, L_1, w_2, and L_2 are identical whether fitting $A(\lambda)$ to eq 14 or $\sigma(\text{total})$ to eq 16. The ratios of C_1/a_1, C_2/a_2, and x/y are all equal to the scaling factor in eq 15, namely $640/(A_{\max} - B)$. The averages of the least-squares parameters for 57 spectra, including the five shown in Figure 5, are reported in Table 1. These 57 spectra, all taken during the same run, were the most consistent of the spectra taken using method 1. These spectra returned constant Gaussian parameters as the trap was warmed, indicating

UV Absorption Spectrum of ClOOCl

J. Phys. Chem. A, Vol. 111, No. 20, 2007 **4327**

TABLE 1: Average Gaussian Parameters and Their Standard Deviations Calculated by Least-Squares Fitting of Eq 16 to 57 Spectra Having A_{max} Greater Than 1[a]

parameter	average	standard deviation	observed range
$C_1/10^{-20}$ cm^2	359.5	0.52	± 20
w_1	294.0	0.85	∓ 5
L_1/nm	244.1	0.01	± 0.1
$C_2/10^{-20}$ cm^2	284.6	0.53	∓ 20
w_2	51.1	0.39	± 1.5
L_2/nm	248.5	0.027	± 1.5

[a] These spectra were all taken during 1 day's run using method 1 to generate dimer. As explained in the text, the last column indicates the approximate range of parameter values observed on four other runs.
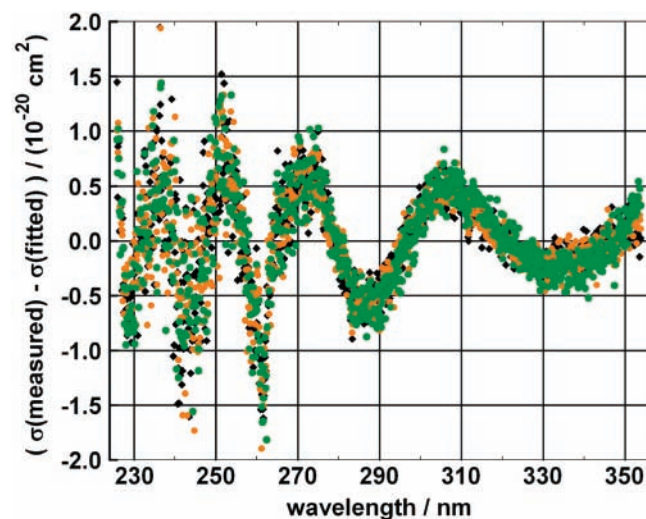

Figure 6. Deviations between the measured and fitted cross sections for three of the spectra of Figure 5. The color coding is the same in both figures.

Figure 7. Same plot as Figure 5, except the lower points show the results of subtracting the contribution of $\sigma(Cl_2)$ from each spectrum.

that no compounds other than ClOOCl and Cl$_2$ were present. For these 57 spectra, the baseline term, B, ranged from -0.018 to -0.011. Fits done with nonconstant baselines, either linear or quadratic in wavelength, gave slightly smaller χ^2 values, but the resulting Gaussian parameters were less consistent than with a constant baseline. Because the largest covariance in the fits was between the baseline (B) and the amount of Cl$_2$ present (x or y), and because blank runs showed very constant baselines for wavelengths longer than 290 nm, these multiparameter baselines were not used. Confidence in the use of a constant B was achieved by its ability to mimic the increased cycling of the room temperature.

The three dotted lines in Figure 5 show the three terms in eq 16 for the least-squares fit to the lowest (green) spectrum. The deviations between the sum of the three dotted lines and the experimental spectrum are shown in Figure 6 as green circles. Most of these deviations are small, less than 1×10^{-20} cm^2, but the pattern of deviations is reproducible as can be seen in Figure 6 for three different spectra. The source of these deviations is not known, but they might be due to the fact that only about 50% of the ClOOCl molecules at 193 K are in their lowest vibrational state.[37] The vibrationally excited molecules will have Franck−Condon factors that differ from those of the ground state and this can influence the absorption spectrum; eq 16 does not address different Franck−Condon factors in the transition.

Using the fitted parameter x in eq 16, it is possible to subtract out the contribution of $\sigma(Cl_2)$ from each spectrum. This has been done in Figure 7 for the same five spectra shown in Figure 5; the lowest curve results from plotting individual points. The
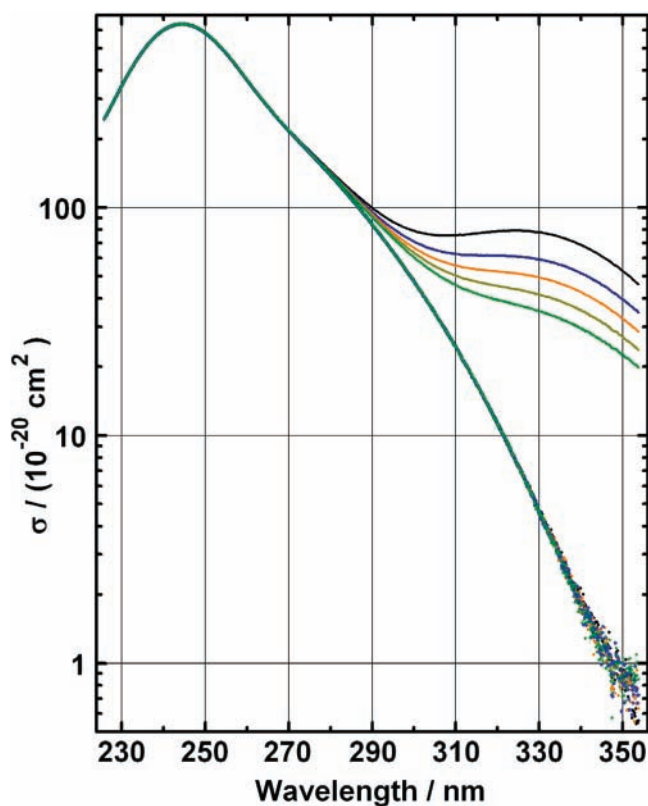
overlap of all five curves is excellent, diverging only when the cross sections approach 1×10^{-20} cm^2. This lower curve is the best current measurement of the spectrum of pure ClOOCl. Equation 17, with parameters taken from Table 1, is the algebraic form of this ClOOCl spectrum, where "2Gauss"

$$\sigma(2\text{Gauss}) = (359.5) \exp(-294[\ln(244.1/\lambda)]^2) + (284.6) \exp(-51.1[\ln(248.5/\lambda)]^2) \quad (17)$$

indicates the use of two Gaussian functions.

For some runs there were drifts of the parameters as the dimer signal grew and then decreased. The limits given in the "observed range" column in Table 1 reflect these variations. These variations were not independent; they covaried so that the overall shape of the absorption changed only slightly. For example, if C_1 drifted, C_2 also changed in such a way that the sum $C_1 + C_2$ remained almost constant. Similarly, if C_1/C_2 increased (or decreased), both L_2 and w_2 increased (or decreased). The order of the $\pm$ or $\mp$ signs in Table 1 is important, and the variations need to be applied simultaneously. These variations in parameters affect the short wavelength cross sections more than those at longer wavelengths.

The cross sections for ClOOCl from this study are given in Table 2. These values have been calculated using eq 17, with small corrections for the average deviations from that equation, as shown in Figure 6. The precision of the cross sections in Table 2, as judged by the reproducibility of the 57 spectra that were used to derive the "average" parameters in Table 1, varies with wavelength. For the short wavelength region, 226−290 nm, a variation of $\pm 0.2\%$ was observed, while for wavelengths longer than 290 nm the standard deviations were approximately $\pm 0.2 \times 10^{-20}$ cm^2.

For the four runs made on other days, which resulted in the "observed range" of parameters listed in Table 1, the uncertain-

TABLE 2: Average Cross Sections of ClOOCl As Determined by Eq 17 and Figure 6[a]

λ	σ(ClOOCl)	λ	σ(ClOOCl)	λ	σ(ClOOCl)
355	0.63	311	22.0	267	252.7
354	0.65	310	23.7	266	265.8
353	0.67	309	25.6	265	279.8
352	0.70	308	27.5	264	295.0
351	0.74	307	29.5	263	311.0
350	0.79	306	31.6	262	327.9
349	0.84	305	33.7	261	346.4
348	0.91	304	36.1	260	367.0
347	0.98	303	38.5	259	388.3
346	1.05	302	41.1	258	410.5
345	1.14	301	43.8	257	433.5
344	1.23	300	46.7	256	456.9
343	1.35	299	49.6	255	480.6
342	1.45	298	52.8	254	504.2
341	1.58	297	56.1	253	527.3
340	1.72	296	59.5	252	549.6
339	1.88	295	63.1	251	569.9
338	2.06	294	66.9	250	588.6
337	2.26	293	70.8	249	604.9
336	2.49	292	74.9	248	618.6
335	2.75	291	79.2	247	629.1
334	3.02	290	83.7	246	636.0
333	3.33	289	88.3	245	639.3
332	3.66	288	93.2	244	638.7
331	4.02	287	98.2	243	634.1
330	4.41	286	103.3	242	625.6
329	4.85	285	108.7	241	613.4
328	5.34	284	114.4	240	597.7
327	5.86	283	120.2	239	578.9
326	6.43	282	126.2	238	558.0
325	7.05	281	132.4	237	532.7
324	7.70	280	138.9	236	506.0
323	8.40	279	145.5	235	478.1
322	9.15	278	152.3	234	449.5
321	10.0	277	159.5	233	420.5
320	10.8	276	167.0	232	391.8
319	11.8	275	174.6	231	363.6
318	12.8	274	182.5	230	336.4
317	13.8	273	190.8	229	310.3
316	15.0	272	199.6	228	285.8
315	16.2	271	208.9	227	263.3
314	17.5	270	218.8	226	242.4
313	18.9	269	229.3		
312	20.4	268	240.6		

[a] The units are nm for λ and (10^{-20} cm^2 molecule^{-1}) for σ. The last digit for each cross section is of marginal significance. The precision of the cross section measurements are observed to be ±0.2% from 230 to 290 nm and $\pm 0.2 \times 10^{-20}$ cm^2 at longer wavelengths. Because these cross sections have been scaled to the average of maximum absolute cross sections reported in the literature, their accuracy is no better than +20% to −10%. The wavelength scale is accurate to ±0.3 nm.

ties were larger, especially at shorter wavelengths. The observed deviations from eq 17 were up to ±9% at 226 nm, ±6% at 230 nm, decreasing to about ±1% at 240, and zero at 244.7 nm, because each spectrum was normalized there. Deviations increased to longer wavelengths, up to ±3% in the 270−310 nm range, and $\pm 1 \times 10^{-20}$ cm^2 at longer wavelengths. The reasons for these variations in cross sections are not known, but certainly a drifting baseline is responsible for some of the deviations at long wavelengths where the absorbances were small. The deviations at the shorter wavelengths are probably due to impurities being present at low enough concentrations so that they are not recognized; evidence for this was the observation that in these runs the fitted parameters drifted as the absorbance changed.

Analysis of the spectra recorded using method 2 to generate the dimer were complicated by the presence of OClO and Cl$_2$O$_3$

as well as Cl$_2$. To apply the method of least squares, it is necessary to have spectra of all of these contaminants. The OClO was synthesized by the standard method, passing a 1% mixture of Cl$_2$ in He through a column containing glass beads and fresh Na(ClO$_2$).[38] Small amounts of OClO diluted in He flowed through the absorption cell cooled to dry ice temperature. The measured absorbance values were scaled to the absolute cross sections of Wahner et al. (1 nm resolution, 204 K) for use in the least-squares calculations.[39] The absolute magnitude of these cross sections are not critical for our procedure because the values used to fit the spectra are also used to subtract out the contributions of OClO.

Finding a reference spectrum for Cl$_2$O$_3$ was more difficult. There is general agreement on the approximate shape of the UV spectrum, with a strong maximum at about 265 nm, but there are serious disagreements about the cross sections, especially at the longer wavelengths. Some of our spectra using method 2 appeared to be mostly Cl$_2$O$_3$ (e.g., spectrum 59 in Figure 3), but they still contained unknown contributions of ClOOCl and Cl$_2$. For the least-squares fitting, we have used the spectra of Burkholder et al.[40] because this seemed to be most consistent with our observations in Figure 3.

Using the reference spectra for Cl$_2$, OClO and Cl$_2$O$_3$, least-squares fits to the experimental spectra were attempted using an equation similar to eq 16, but with two additional fitted variables for the contributions due to OClO and Cl$_2$O$_3$. There were now ten variables to be determined, three for each Gaussian, one each for contributions of Cl$_2$, OClO, and Cl$_2$O$_3$ and one baseline term. For the spectra with only small amounts of Cl$_2$O$_3$, which were most useful for determining the long wavelength part of the dimer spectrum, the fits converged slowly or not at all, and the fitted constants were inconsistent from spectrum to spectrum. The main trouble appeared to be the large covariance between the coefficient for the amount of Cl$_2$O$_3$ and the parameters of the second (longer wavelength) Gaussian for ClOOCl. A small bulge on the long wavelength side of the dimer spectrum (e.g., spectrum 36 in Figure 3) can be fit by a small contribution of Cl$_2$O$_3$, or by increasing the amplitude and width of the second Gaussian, or by a combination of both. Because of the convergence difficulties and the inconsistencies, this approach was abandoned.

The main purpose of using method 2 is to establish if the dimer spectrum consists of just the two Gaussians determined using method 1, or whether there is an additional electronic transition that looks so similar to the chlorine spectrum that it can be mistaken for a Cl$_2$ impurity. Instead of attempting to redetermine the six parameters of the two Gaussians, we have applied eq 18 to fit the absorbances in method 2 spectra. Here

$$A(\lambda) = d_1\sigma(2\text{Gauss}) + d_2\sigma(\text{Cl}_2\text{O}_3) + d_3\sigma(\text{OClO}) + d_4\sigma(\text{Cl}_2) + B \quad (18)$$

σ(2Gauss) is given by eq 17, the cross sections for Cl$_2$ are from eq 13, and the cross sections for OClO and Cl$_2$O$_3$ are represented by columns of numbers in the least-squares fitting routine. Least-squares fitting of method 2 spectra to eq 18 converged rapidly.

There are two complications in applying eq 18 to the spectra of method 2. Because the amount of ClOOCl collected using method 2 was considerably smaller than that from method 1, the maximum absorbances were less, typically 0.5 instead of 1.5−2.5. The region of critical interest is for λ > 300 nm, which then involved absorbances of 0.05−0.01. Also, the amounts of Cl$_2$ were smaller in method 2 and, consequently, the covariance

between parameters d_4 and B in eq 18 became quite large. This problem was minimized by a two-step procedure. First, eq 18 was fit to the full data set (1024 points) and the resulting coefficient d_2 was used to subtract out the contribution of Cl_2O_3. The resulting data set was then truncated to 511 points ($\lambda >$ 290 nm) and refit to eq 19, which is similar to eq 18 but without the term $d_2\sigma(Cl_2O_3)$. The parameters d_1 and d_3 were similar in fitting eq 18 or 19, but the parameters d_4 and B changed significantly.

$$A(\lambda) = d_1\sigma(2\text{Gauss}) + d_3\sigma(\text{OClO}) + d_4\sigma(Cl_2) + B \quad (19)$$

As a test of the reasonableness of the fit, the terms $d_1\sigma(2\text{Gauss})$, $d_3\sigma(\text{OClO})$, and B were subtracted from the truncated data set and the remainder was plotted as a function of wavelength. Using the results from fitting eq 19 to the truncated data set gave a weak spectrum with a maximum at 330 nm, consistent with the presence of Cl_2 and the results of method 1. Applying the same stripping procedure to the results of fitting eq 18 to the full data set gave residuals that did not always look like Cl_2, and in several cases resulted in negative absorbances. Use of the truncated data set and eq 19 appears to result in a baseline correction, B, that is more realistic for the weak signals at long wavelengths.

Absorbances from method 2 were converted to cross sections using a procedure similar to that used for method 1. Although neither OClO nor Cl_2 absorb appreciably at 245 nm, Cl_2O_3 does.[40] Consequently, it was necessary to consider the contribution of Cl_2O_3 to the maximum so that when its contribution is subtracted, the remaining spectrum has a maximum cross section of 640. Instead of eq 15, eq 20 was used to convert method 2 absorbances to cross sections, where d_2/d_1 represents the fitted molecular ratio of Cl_2O_3/ClOOCl using the full data set, 989 is the cross section of Cl_2O_3 at 245 nm, and $A(244.7)$ is the measured absorbance at 244.7 nm. Figure 8 shows an example of this procedure applied to a truncated spectrum.

$$\sigma(\text{total}) = \frac{(640 + 989d_2/d_1)(A(\lambda) - B)}{(A(244.7) - B)} \quad (20)$$

Discussion

The current spectrum of ClOOCl reported in Table 2 agrees best with the spectrum reported previously by Huder and DeMore.[7] Because both have been normalized to 640 at about 245 nm, they can be compared directly. The two spectra agree to within 1% from 240 to 260 nm but diverge at both shorter and longer wavelengths, disagreeing by 9% at 226 nm, 10% at 300 nm, and 30% at 310 nm. At each wavelength, the Huder and DeMore cross sections are larger than those in Table 2. At wavelengths longer than 310 nm, Huder and DeMore proposed a log-linear extrapolation that rapidly diverges from the values in Table 2, becoming 4 times larger by 340 nm. The cross sections reported by Burkholder et al.[6] are even larger than those of Huder and DeMore in the region >245 nm; compared to Table 2, they are twice as large at 300 nm and more than 9 times larger at 340 nm. Because other literature values fall between those of Burkholder et al. and Huder and DeMore, it is clear that the σ(ClOOCl) in Table 2 are significantly below the currently recommended values[18] in the region of most importance to the atmosphere, namely for $\lambda >$ 300 nm.

Although there is general agreement in the literature on the features of the ClOOCl spectrum, with a peak near 245 nm and a tail to longer wavelengths, there is only modest agreement on the absolute cross sections. Cox and Hayman[5] used mass
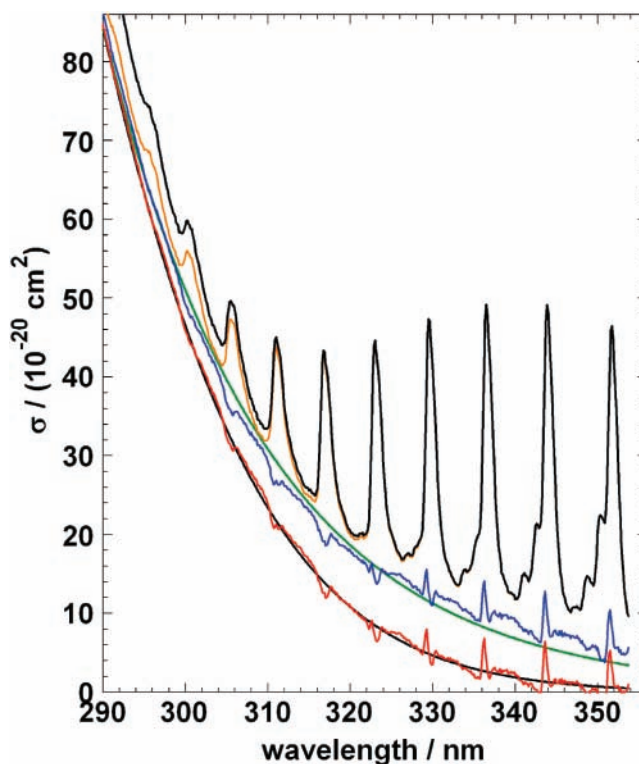

Figure 8. Spectrum using method 2 to generate ClOOCl. Conditions: 1.5 Torr CF_2Cl_2; 2.1 Torr O_3; 152 Torr CF_4; balance He. The spectrum (black line) has been normalized to 653 at 244.7 nm using eq 20. The colored lines result from sequentially subtracting the impurities (values in parentheses give the ratio of the impurity to ClOOCl): orange, Cl_2O_3 (0.0136); blue, OClO (0.0359); red, Cl_2 (0.281). The smooth green line represents the ClOOCl cross sections suggested by Huder and DeMore and the smooth black line is eq 17 derived from method 1 spectra.

balance to derive a cross section at the peak, σ_{max}, of 640 ± 60 (all times 10^{-20} cm^2). DeMore and Tschuikow-Roux[8] compared the loss of reactant Cl_2O with the formation of ClOOCl and concluded that σ_{max} was 680 ± 80. Burkholder et al.[6] used mass balance to determine a σ_{max} of 650 with unsymmetrical error limits of +80 and −50. For the present study, we have decided to use the σ_{max} recommended by the JPL/NASA evaluation,[18] namely 640, with the understanding that if future studies establish a more reliable value, all of our absolute cross sections should be scaled accordingly. The above error estimates suggest that the uncertainty in all of the cross sections in Table 2 may be as great as +20% or −10%.

Analysis of the spectra measured in this study suggests that the main ClOOCl absorption consists of two electronic transitions, one centered at 244.1 nm (5.08 eV) and the other at 248.5 nm (4.99 eV). Although the energies of the transitions are very similar, the widths of the bands differ by a factor of 2.5, which implies that the slopes of the excited-state potential energy surfaces (PES) differ significantly. One expects the broader band to be a transition to a steep PES because the Franck−Condon overlap will be large over a range of energies. Conversely, the narrower band would involve a flatter PES where good Franck−Condon overlap occurs only within a narrow energy range.

These observations are consistent with several ab initio calculations on ClOOCl. Stanton and Bartlett[41] and also Peterson and Francisco[42] find a total of eight allowed electronic transitions in the region below 6 eV. These eight are grouped into four pairs, with each pair having similar energies. The pairing occurs because the ClOOCl molecule has a C_2 axis of symmetry and the excitations are largely to Cl−O antibonding σ^* orbitals. As a result, the excited-state wavefunctions need to be either

TABLE 3: Comparison of Theoretical Predictions of Energies and Oscillator Strengths of the Third Pair of States with Present Experimental Values

references	energies/eV	oscillator strengths, f
Stanton and Bartlett[41]	5.42, 5.41	0.014, 0.079
Peterson and Francisco[42]	5.82, 5.78	0.018, 0.092
Toniolo et al.[44]	5.36, 4.92	0.0027, 0.042
Kaledin and Morokuma[45]	5.22, 4.58	0.017, 0.032
present exptl values	5.08, 4.99	0.017, 0.032

symmetric or antisymmetric with respect to the symmetry operation. The splittings between the pairs of symmetric/antisymmetric states in these two studies are calculated to be quite small, in the range 0−0.05 eV. These two studies also calculate oscillator strengths, and they agree that transitions to the third pair of states, $4(^1A)$ and $3(^1B)$, are the strongest.

For an absorption that can be fitted to the Gaussian function used here, it is possible to calculate the oscillator strength, f, of the transition using eq 21, where ϵ_o is the electric constant, m_e

$$f = \frac{4\epsilon_0 m_e c^2 \sigma_{\max} \pi^{1/2} \exp(1/4w)}{e^2 w^{1/2} \lambda_{\max}} \quad (21)$$

and e are the mass and charge of an electron, and c is the speed of light.[29] Using the average parameters reported in Table 1 ($\sigma_{\max} = C_1$ or C_2, $w = w_1$ or w_2, and $\lambda_{\max} = L_1$ or L_2), the oscillator strengths are calculated to be 0.017 and 0.032 for the 244.1 and 248.5 nm bands, respectively. These f values are similar to those calculated for the $4(^1A)$ and $3(^1B)$ states.

Two other theoretical calculations reach slightly different conclusions. Toniolo et al. and Kaledin and Morokuma agree that at least one of the transitions to the third pair of states is strong,[43−45] but they both find that the splitting between the $4(^1A)$ and $3(^1B)$ states is larger, approximately 0.4−0.6 eV. The PES calculated by Toniolo et al. (Figure 2 of ref 44) indicates several avoided crossings in the vicinity of 5 eV, which give rise to quite different slopes in the excited states. This could account for the different band widths observed. These theoretical results are collected in Table 3 together with the experimental values of the present study. While none of the ab initio studies give perfect agreement with the observed spectra, taken together they provide good theoretical support for the present interpretation that the ClOOCl spectrum consists of two electronic transitions having similar energies but different band widths.

The ClOOCl cross sections of most importance to modeling atmospheric ozone concentrations are those at wavelengths longer than 300 nm. This is just the region that suffers the most interference in the above spectra. Especially troubling is the observation of method 1 spectra that although the Cl$_2$/ClOOCl ratio decreases significantly as the trap warms, the ratio never gets much below unity as the last of the dimer evaporates. Could it be that there is another electronic transition, or transitions, in ClOOCl that appear so similar in shape to the Cl$_2$ absorption that we and others have mistakenly subtracted it out?

This important question can be addressed by the spectra taken using method 2. Figure 8 shows the long wavelength portion of a spectrum from a CF$_2$Cl$_2$/O$_3$/CF$_4$ mixture; the presence of 21% CF$_4$ reduces, but does not eliminate, the presence of OClO and Cl$_2$O$_3$. This spectrum, with a maximum absorbance of 0.4, was fit using the two step procedure described above. Knowing the amounts of impurities in the spectrum, it is possible to subtract them out. The contribution of Cl$_2$O$_3$ is quite small and is confined mostly to the region $\lambda < 310$ nm. Subtracting the

contribution of OClO gives the blue line in Figure 8; the residual structure is because of a slight mismatch in the wavelength scales of the experimental and reference spectra, caused by subpixel wavelength shifts due to the temperature related compression/expansion of the spectrometer. And, finally, the contribution of Cl$_2$ is subtracted to give the red line. For comparison the lower black line is σ(2 Gauss) in this wavelength range and the solid green line is the extrapolated cross sections suggested by Huder and DeMore.[7]

Two observations are important in Figure 8. First, when all the known impurities are subtracted, the resulting red line agrees well with σ(2 Gauss) derived from method 1; the experimental data are compatible with the assumptions underlying eqs 18 and 19. Second, the results of subtracting out the contributions of Cl$_2$O$_3$, which is very minor in this region, and OClO, which can be done with the least uncertainty because of the structured nature of its spectrum, should give an *upper limit* to the cross sections for ClOOCl. As can be seen, the blue line in Figure 8 falls close to the extrapolated cross sections suggested by Huder and DeMore. If ClOOCl has additional electronic transitions in this region, they contribute no more than about 8 units at 330 nm, because σ(2Gauss) contributes about 5 to this upper limit of 13. It is concluded that as an *upper limit*, the cross sections of ClOOCl at wavelengths longer than 310 nm cannot be much larger than the extrapolation suggested by Huder and DeMore.[7]

The molecular ratio of Cl$_2$ to ClOOCl suggested by the analysis in Figure 8, 0.28, is a factor of 3−4 lower than the limiting values observed using method 1. It is reasonable that there is some Cl$_2$ present when using method 2 to generate ClOOCl. Modeling showed that even if the gas mixture was exposed to a single laser pulse, this ratio would be at best about 0.06, due to the overlap between the decaying Cl concentration and the growing ClOOCl concentration. Because of diffusion and non-plug flow at the exit of the photolysis cell, some dimer must remain in the cell when the next laser pulse arrives, allowing reaction 5 to generate additional Cl$_2$. And, finally, ClOOCl is a fragile molecule, prone to photolysis by the analysis beam and to decomposition on the walls of the absorption cell during its 90 s residence time. We conclude that Figure 8 is strong support for assigning the spectrum of ClOOCl in this wavelength region to σ(2Gauss).

Another approach to the question of additional electronic transitions of ClOOCl is to extend the absorbance measurements to longer wavelengths to establish a more reliable baseline. Figure 9 shows three spectra obtained using method 1. The absorbances have been converted to cross sections by using the measured absorbances at 281 and 330 and assuming that only σ(2Gauss) and σ(Cl$_2$) contribute. The resulting molecular ratios of Cl$_2$/ClOOCl are 4.46, 1.86, and 1.13 for the top three curves. Subtracting out each of the contributions of chlorine results in the lowest curve, which is actually three overlapping curves. This lower curve coincides with σ(2Gauss), shown as diamonds, within the experimental uncertainties. Additional spectra measuring out to 498 nm show no absorptions except for the long wavelength tail of Cl$_2$. If there is another electronic transition of ClOOCl in this wavelength region, it must have a shape that is essentially identical to that of Cl$_2$. The more likely interpretation, in our opinion, is that there is no significant ClOOCl absorption in the long wavelength region except for the tail of σ(2Gauss).

It should be noted here that the middle (blue) spectrum in Figure 9 is based on the same data set as the black spectrum in Figure 4. The blue dots in Figure 9, which result from subtracting 1.86 times σ(Cl$_2$) from the blue spectrum, correspond

UV Absorption Spectrum of ClOOCl

J. Phys. Chem. A, Vol. 111, No. 20, 2007 **4331**
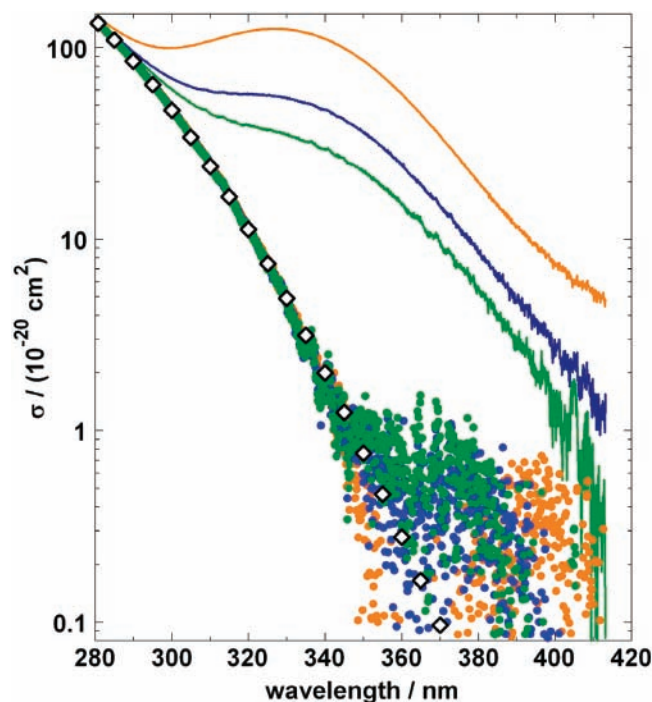

Figure 9. Cross sections at longer wavelengths for three spectra using method 1 to generate ClOOCl. Conditions as in Figure 2. The fitted ratios of Cl_2/ClOOCl are 4.46, 1.86, and 1.13 for the top three spectra. Using the same color code, the lower points result from subtracting out the contributions from $\sigma(Cl_2)$. The open diamonds are $\sigma(2Gauss)$ from eq 17.

TABLE 4: Summary of Calculated Photolysis Rates for Chlorine Peroxide Using Different Determinations of the Absorption Cross Sections[a]

cross sections from	photolysis rate/s^{-1}	ratio to this study
Burkholder[6]	13.2×10^{-4}	8.9
Huder and DeMore[7]	5.13×10^{-4}	3.5
JPL 2006[18]	9.17×10^{-4}	6.2
present study	1.48×10^{-4}	1

[a] Atmospheric conditions are given in the text.

closely to the next to lowest (brown) curve in Figure 4, which corresponds to subtracting the equivalent of 1.8 times $\sigma(Cl_2)$ from the black spectrum. Thus the method of least-squares fitting of the data provides a quantitative answer to the question, posed earlier, of how much chlorine to subtract and it avoids the subjectivity of the manual subtraction method.

Atmospheric Implications

To assess the impact of the new chlorine peroxide cross sections, photolysis rates were calculated for the Arctic polar vortex, at a solar zenith angle of 86°, 20 km altitude, and O_3 and temperature profiles measured in March 2000.[46] Figure 10 shows the calculated wavelength-dependent partial photolysis rates for this study compared to the work of Burkholder et al.,[6] Huder and DeMore,[7] and the current NASA recommendation (JPL 2006).[18] A comparison of these relevant cross sections is given in Figure S1 in the Supporting Information.

Figure 10 illustrates the importance of the long wavelength cross sections. The increasing magnitude of the solar flux at longer wavelengths makes an accurate determination of the increasingly small cross sections essential. The corresponding photolysis rates are given in Table 4, along with their ratios to the current determination.
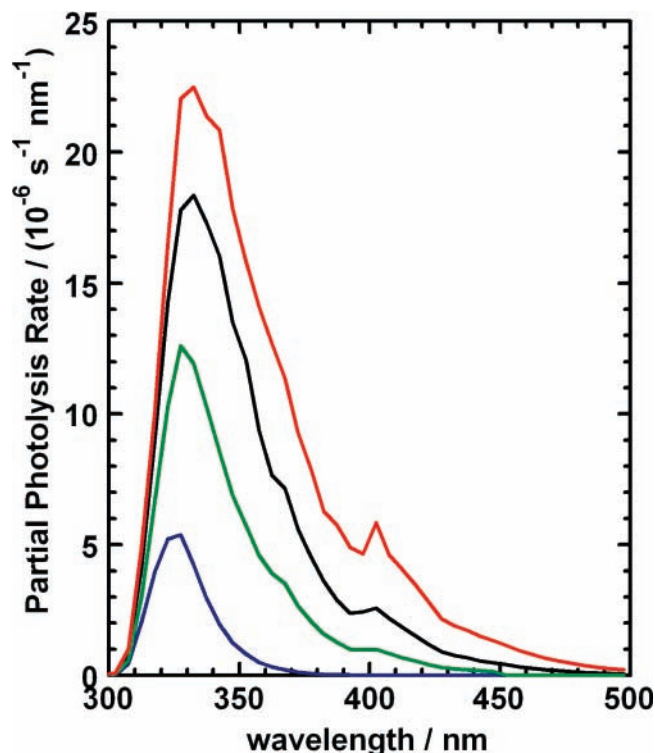

Figure 10. Partial photolysis rates of ClOOCl in the atmosphere calculated for different cross sections. Conditions: altitude 20 km; solar zenith angle 86°; O_3 concentrations and temperature values measured in the polar vortex for March 2000.[46] Cross sections: Burkholder et al. (red);[6] JPL 2006 (black);[18] Huder and DeMore (green);[7] present values (blue).

The results of this study are in major disagreement with recent conclusions of various modeling and field work studies,[9−12] which find good agreement only when using the extrapolated cross sections of Burkholder et al. The calculated photolysis rate differs between the two studies by a factor of about 9 (Table 4). This difference will be further enhanced at higher solar zenith angles. Because photolysis of ClOOCl is the rate limiting step in the loss of polar ozone, the adoption in atmospheric models of the cross sections determined in the present study will lead to a large reduction in the calculated chemical ozone depletion. New photolytic and/or reactive pathways will be required to obtain closer agreement between models and measurements.

Supporting Information Available: Figure showing the comparison of the ClOOCl cross sections most relevant for stratospheric modeling. This material is available free of charge via the Internet at http://pubs.acs.org.

References and Notes

(1) Molina, L. T.; Molina, M. J. *J. Phys. Chem.* **1987**, *91*, 433.
(2) Molina, M. J.; Colussi, A. J.; Molina, L. T.; Schindler, R. N.; Tso, T. L. *Chem. Phys. Lett.* **1990**, *173*, 310.

(3) Moore, T. A.; Okumura, M.; Seale, J. W.; Minton, T. K. *J. Phys. Chem. A* **1999**, *103*, 1692.

(4) Plenge, J.; Flesch, R.; Kühl, S.; Vogel, B.; Müller, R.; Stroh, F.; Rühl, E. *J. Phys. Chem. A* **2004**, *108*, 4859.

(5) Cox, R. A.; Hayman, G. D. *Nature* **1988**, *332*, 796.

(6) Burkholder, J. B.; Orlando, J. J.; Howard, C. J. *J. Phys. Chem.* **1990**, *94*, 687.

(7) Huder, K. J.; DeMore, W. B. *J. Phys. Chem.* **1995**, *99*, 3905.

(8) DeMore, W. B.; Tschuikow-Roux, E. *J. Phys. Chem.* **1990**, *94*, 5856.

(9) Stimpfle, R. M.; Wilmouth, D. M.; Salawitch, R. M.; Anderson, J. G. *J. Geophys. Res.* **2004**, *109*, doi:10.1029/2003JD003811.

(10) Frieler, K.; Rex, M.; Salawitch, R. M.; Canty, T.; Striebel, M.; Stimpfle, R. M.; Pfeilsticker, K.; Dorf, M.; Weisenstein, D. K.; Godin-Beekmann, S. *Geophys. Res. Lett.* **2006**, *33*, doi:10.1029/2005GL025466.

(11) Von Hobe, M.; Grooss, J.-U.; Müller, R.; Hrechanyy, S.; Winkler, U.; Stroh, F. *Atmos. Chem. Phys.* **2005**, *5*, 693.

(12) Chipperfield, M. P.; Feng, W.; Rex, M. *Geophys. Res. Lett.* **2005**, *32*, doi:10.1029/2005GL022674.

(13) Bloss, W. J.; Nickolaisen, S. L.; Salawitch, R. J.; Friedl, R. R.; Sander, S. P. *J. Phys. Chem. A* **2001**, *105*, 11226.

(14) Ingham, T.; Sander, S. P.; Friedl, R. R. *Faraday Discuss.* **2005**, *130*, 89.

(15) Birk, M.; Friedl, R. R.; Cohen, E. A.; Pickett, H. M.; Sander, S. P. *J. Chem. Phys.* **1989**, *91*, 6588.

(16) Slanina, Z.; Uhlik, F. *J. Phys. Chem.* **1991**, *95*, 5432.

(17) Stanton, J. F.; Rittby, C. M. L.; Bartlett, R. J.; Toohey, D. W. *J. Phys. Chem.* **1991**, *95*, 2107.

(18) Sander, S. P.; Ravishankara, A. R.; Golden, D. M.; Kolb, C. E.; Kurylo, M. J.; Molina, M. J.; Moortgat, G. K.; Finlayson-Pitts, B. J.; Wine, P. H.; Huie, R. E.; Orkin, V. L. Chemical Kinetics and Photochemical Data for Use in Atmospheric Studies, Evaluation Number 15. Jet Propulsion Laboratory: Pasadena, CA, 2006.

(19) Wine, P. H.; Ravishankara, A. R. *Chem. Phys.* **1982**, *69*, 365.

(20) Matsumi, Y.; Comes, F. J.; Hancock, G.; Hofzumahaus, A.; Hynes, A. J.; Kawasaki, M.; Ravishankara, A. R. *J. Geophys. Res.* **2002**, *107*, 4024.

(21) Takahashi, K.; Wada, R.; Matsumi, Y.; Kawasaki, M. *J. Phys. Chem.* **1996**, *100*, 10145.

(22) Orlando, J. J.; Tyndall, G. S.; Wallington, T. J.; Dill, M. *Int. J. Chem. Kinet.* **1996**, *28*, 433.

(23) Orlando, J. J.; Tyndall, G. S.; Wallington, T. J. *J. Phys. Chem.* **1996**, *100*, 7026.

(24) McGivern, W. S.; Kim, H. J.; Francisco, J. S.; North, S. W. *J. Phys. Chem. A* **2004**, *108*, 7247.

(25) Bayes, K. D.; Friedl, R. R.; Sander, S. P. *J. Phys. Chem. A* **2005**, *109*, 3045.

(26) Nölle, A.; Heydtmann, H.; Meller, R.; Schneider, W.; Moortgat, G. K. *Geophys. Res. Lett.* **1992**, *19*, 281.

(27) McKeachie, J. R.; Appel, M. F.; Kirchner, U.; Schindler, R. N.; Benter, T. *J. Phys. Chem. B* **2004**, *108*, 16786.

(28) Maric, D.; Burrows, J. P.; Meller, R.; Moortgat, G. K. *J. Photochem. Photobiol. A Chem.* **1993**, *70*, 205.

(29) Maric, D.; Burrows, J. P. *J. Phys. Chem. A* **1996**, *100*, 8645.

(30) Maric, D.; Burrows, J. P.; Moortgat, G. K. *J. Photochem. Photobiol A Chem.* **1994**, *83*, 179.

(31) Ingham, T.; Bauer, D.; Landgraf, J.; Crowley, J. N. *J. Phys. Chem. A* **1998**, *102*, 3293.

(32) Fahr, A.; Nayak, A. K.; Huie, R. E. *Chem. Phys.* **1995**, *199*, 275.

(33) Lightfoot, P. D.; Cox, R. A.; Crowley, J. N.; Destriau, M.; Hayman, G. D.; Jenkin, M. E.; Moortgat, G. K.; Zabel, F. *Atmos. Environ.* **1992**, *26A*, 1805.

(34) Crowley, J. N.; Moortgat, G. K. *J. Chem. Soc., Faraday Trans.* **1992**, *88*, 2437.

(35) Catoire, V.; Lesclaux, R.; Lightfoot, P. D.; Rayez, M.-T. *J. Phys. Chem.* **1994**, *98*, 2889.

(36) Maric, D.; Crowley, J. N.; Burrows, J. P. *J. Phys. Chem. A* **1997**, *101*, 2561.

(37) Plenge, J.; Kühl, S.; Vogel, B.; Müller, R.; Stroh, F.; von Hobe, M.; Flesch, R.; Rühl, E. *J. Phys. Chem. A* **2005**, *109*, 6730.

(38) Derby, R. I.; Hutchinson, W. S. *Inorg. Synth.* **1953**, *4*, 152.

(39) Wahner, A.; Tyndall, G. S.; Ravishankara, A. R. *J. Phys. Chem.* **1987**, *91*, 2734.

(40) Burkholder, J. B.; Mauldin, R. L.; Yokelson, R. J.; Solomon, S.; Ravishankara, A. R. *J. Phys. Chem.* **1993**, *97*, 7597.

(41) Stanton, J. F.; Bartlett, R. J. *J. Chem. Phys.* **1993**, *98*, 9335.

(42) Peterson, K. A.; Francisco, J. S. *J. Chem. Phys.* **2004**, *121*, 2611.

(43) Toniolo, A.; Persico, M.; Pitea, D. *J. Phys. Chem. A* **2000**, *104*, 7278.

(44) Toniolo, A.; Granucci, G.; Inglese, S.; Persico, M. *Phys. Chem. Chem. Phys.* **2001**, *3*, 4266.

(45) Kaledin, A. L.; Morokuma, K. *J. Chem. Phys.* **2000**, *113*, 5750.

(46) Salawitch, R. J.; Canty, T. Personal communication.